Colloid and Polymer Science (2021) 299:1–10
https://doi.org/10.1007/s00396-020-04761-x

ORIGINAL CONTRIBUTION

A nanocomposite interpenetrating hydrogel with high toughness: effects of the posttreatment and molecular weight

Chao Niu[1] · Huijuan Zhang[1] · Biao Yang[1]

Received: 23 January 2020 / Revised: 4 September 2020 / Accepted: 27 September 2020 / Published online: 10 October 2020

Abstract

Previously, we prepared a tough nanocomposite interpenetrating hydrogel by chemical crosslinking of acrylamide (AM) with vinyl-modified silica nanoparticles (VSNPs), combined with physical crosslinking of polyvinyl alcohol (PVA). It is well-known that posttreatment method and molecular weight play important roles in the mechanical properties of the tough hydrogels. In this paper, different post-treatment methods, i.e., freeze-thaw and annealing-swelling and varying PVA degree of polymerization (500 and 1700) were used to prepare the nanocomposite interpenetrating hydrogels. The effects of posttreatment and PVA molecular weight on the mechanical and swelling properties were investigated in detail. Tensile tests showed that annealing-swelling process exerted a more pronounced influence on elevating the tensile strength of nanocomposite interpenetrating hydrogels, which arose from the increased crystallization degree of PVA and the denser network. Hydrogels with lower PVA molecular weight have higher tensile strength after freeze-thaw cycle than that with higher PVA molecular weight. Cyclic loading–unloading tests revealed that the gels with lower molecular weight of PVA can dissipate higher energy at 100% strain. The swelling kinetic study revealed that the swelling behaviors of nanocomposite interpenetrating hydrogels followed the pseudo-second-order dynamic equation.

Keywords Hydrogels · Nanocomposites · Swelling behavior

Introduction

Hydrogels have drawn much attention and interest due to their unique properties, and have been used in drug delivery [1–3], tissue engineering [4–6], sensors [7–9], and so on. Traditional hydrogels suffer from lower strength and toughness, and their potential applications as mechanic device have been limited to a large extent. To overcome this shortcoming, a large amount of mechanically strong gels have been developed, including topological (TP) hydrogels [10–14], nanocomposite (NC) hydrogels [15–18], and double network (DN) hydrogels [19–23]. The reinforcement of these tough hydrogels is usually realized by modulating the inherent characteristic of polymer matrixes, crosslinking manners, or preparation methods.

Polyvinyl alcohol (PVA) is one of the nontoxic, environmentally friendly, biodegradable, and water-soluble polymers [24]. PVA-based double-network hydrogels have been extensively applied for various fields [25, 26]. The vast number of hydroxyl side groups in PVA not only makes it hydrophilic but also allows this polymer to form a semicrystalline structure through intramolecular hydrogen bonding [27, 28]. In many cases, physical method such as freeze-thaw cycle was preferred to prepare PVA hydrogels since no toxic crosslinking agent is needed [29–32]. In the cycle, ice crystal forms when PVA solution is frozen, which expels PVA to phase-separate and promotes the formation of concentrated domains of PVA. After thawing, these aggregated PVA domains are free to form hydrogen bonds and crystals, and physically crosslinked gel is formed. Alternatively, PVA physical hydrogels could be formed by an anneal-swelling treatment as found by Ikada et al. [33]. Annealing treatment can promote formation of hydrogen bonds, leading to crystallization of PVA. In PVA-based tough hydrogels, PVA plays an important role since it can generate a large number of crystallites to serve as physical crosslinks, which significantly affect performance of resulting hydrogels [34].

In our previous study [35], a tough nanocomposite interpenetrating hydrogel was successfully fabricated with dual

✉ Huijuan Zhang
zhanghuijuan@btbu.edu.cn

[1] School of Material and Mechanical Engineering, Beijing Technology and Business University, Beijing 100048, China

crosslinkers: one was chemical crosslinking of acrylamide (AM) monomers with vinyl-modified silica nanoparticles (VSNPs); the other was the physical crosslinking of PVA owing to the freeze-thaw cycle. Thanks to the nanoreinforcement and the physical crosslinker, the nanocomposite interpenetrating hydrogel showed excellent tensile strength with good recovery. Anneal-swelling has been proven to be an alternative and probably more effective strategy to strengthen the PVA-incorporating hydrogel [33]. Moreover, the degree of polymerization of polymers can also exert a remarkable influence on the tensile properties of the tough gels [36–38]. In this work, two posttreatment methods, i.e., freeze-thaw and annealing-swelling, were utilized to produce nanocomposite interpenetrating hydrogels, and the mechanical and swelling properties were investigated in detail. The effect of PVA molecular weight on the tensile strength and swelling behaviors of nanocomposite interpenetrating hydrogels was also discussed. X-Ray diffraction (XRD) and scanning electron microscope (SEM) were performed to clarify the structure-property relationship of the gels.

Experimental section

Chemicals

Acrylamide (AM), *N, N*-methylene bisacrylamide (BIS), ammonium persulfate (APS), and vinyl triethoxysilane were purchased from Guoyao Group Chemical Reagent Co., Ltd. Polyvinyl alcohols (PVA-1799, PVA-105, with degree of polymerization of 1700 and 500 and alcoholysis degree 99%) were purchased from Changchun Chemical Co., Ltd.

Sample preparation

Synthesis of VSNPs

The vinyl hybrid silica nanoparticles were synthesized according to the literature [39, 40]. Vinyl triethoxysilane (3.8 g) and deionized water (30 g) were mixed in a flask and mechanically stirred for about 12 h until the oily droplets disappeared. The transparent vinyl-modified SiO_2 nanoparticles suspension (VSNPs) was obtained.

Preparation of nanocomposite interpenetrating hydrogels

The nanocomposite interpenetrating hydrogels were prepared by a two-step procedure. Take PVA1799 as an example. Firstly, 15 wt% PVA-1799 aqueous solution was prepared by dissolving 15 g PVA into 85-g deionized water at 90 °C under stirring. Then the mixture solution was cooled to room temperature. Afterwards, 3-g AM and 5-mL 1.5 wt% diluted aqueous VSNPs dispersion synthesized previously (weight percent with respect to AM) were added into 10-mL 15 wt% PVA aqueous solution under vigorous stirring until the components were completely mixed. Then, 30-mg APS was added into the above solution and stirred for 30 min. Finally, the solution was transferred into a mold. The radical polymerization occurred at 80 °C for 6 h. In this step, a VSNPs crosslinked hydrogel was formed. In order to obtain hydrogels with different properties, synthetic hydrogels were treated with different processing: (a) control; (b) freeze-thawing; and (c) anneal-swelling. Freeze-thawed gels were subjected to 4 h of freezing at − 20 °C and 6 h of thawing at 25 °C for 1 cycle, marked as PVAx-freeze gels. Anneal-swelled hydrogels were prepared by drying at 80 °C for 3 h and annealing at 120 °C for 1 h, and subsequently immersed in distilled water at room temperature until their weight became constant, marked as PVAx-annealing gels. In both gels, x represents the PVA grade. The general procedure used to prepare the nanocomposite interpenetrating hydrogels is illustrated in Scheme 1. The detailed sample composition and preparation condition are shown in Table 1 as below.

Characterization and tests

Dynamic light scattering

Dynamic light scattering (DLS) was measured using a commercial spectrometer (Zetasizer Nano ZS, Marvin) equipped with a 22 mW He-Ne laser ($\lambda_0 = 632.8$ nm) as the light source. In DLS experiments, scattering light was collected at a fixed angle of 90° at 25 °C.

FT-IR analysis

FT-IR was measured using a commercial spectrometer (Nicolet iS10 FT-IR spectrometer, Nicolli USA). In infrared test, range of waves was 400–4000 cm^{-1}; spectrometer resolution was 4 cm^{-1}; signal to noise was 50,000:1 and scanning 32 times.

X-ray diffraction

X-ray diffraction (XRD) patterns were carried out on the samples in reflection mode ($2\theta = 10–50°$) using an X'pert Powder (PANalytical, Netherlands) with CuKα ($\lambda = 0.1542$ nm) radiation generated at 40 kV and 200 mA.

Scanning electron microscope

The internal network morphologies of the hydrogels were observed by scanning electron (SEM) (QUANTA FEG 250). The hydrogel samples were freeze-dried for SEM observation.

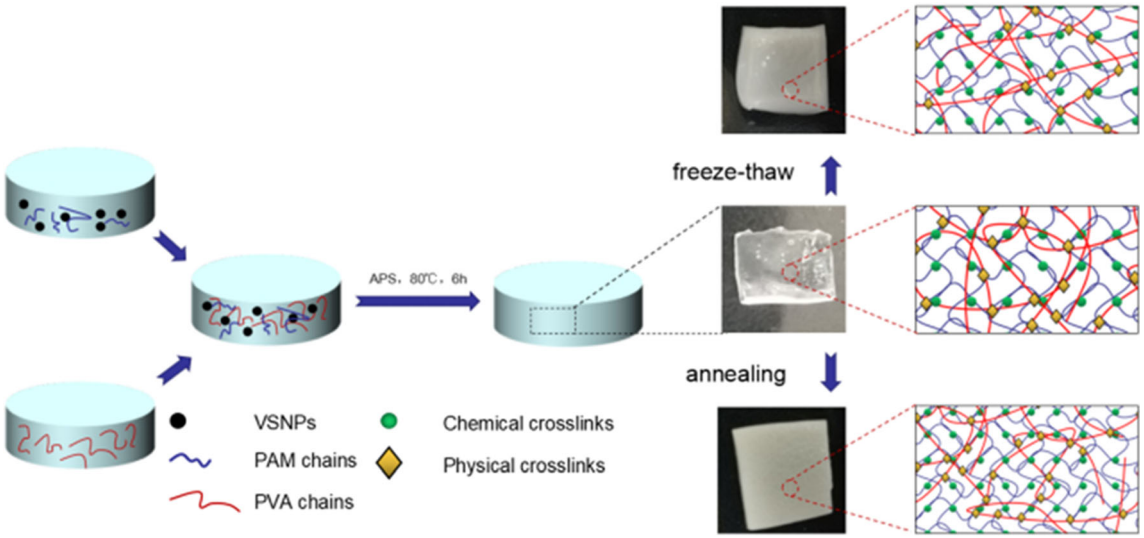

Scheme 1 Schematic preparation process of nanocomposite interpenetrating hydrogel

Mechanical properties test

The tensile and hysteresis measurements of the hydrogels were conducted by using a TA.XT Plus texture analyzer (Stable Micro Systems, UK). After a specific posttreatment, the sample was cut into a dumbbell (length 35 mm, width 4 mm) using a particular specification of the cutter. The thickness of the three layers of the spline was measured with a caliper. The average value was recorded and used. Both ends of the dumbbell-shaped sample were connected to the clamps with the lower clamp fixed. The upper clamp was pulled by the load cell at a constant velocity of 100 mm min^{-1} at room temperature, by which the stress–strain curve was recorded. In a hysteresis measurement, a dumbbell-shaped sample was first elongated to a predetermined maximum stretch and then unloaded to zero force at a constant velocity of 100 mm min^{-1}. The dissipated energy for each cycle, ΔU, is defined as the area of hysteresis loop encompassed by the loading–unloading curve.

$$\Delta U = \int_{\text{loading}} \sigma d\varepsilon - \int_{\text{unloading}} \sigma d\varepsilon \quad (1)$$

Determination of swelling ratio

The swelling ratio (SR) of a given sample was measured as follows. Firstly, a completely dried sample was immersed into distilled water at ambient temperature. Then the samples were taken out and weighed after gentle surface wiping using absorbent paper at regular time intervals. The swelling ratio was calculated according to the following equation. All the measurements were carried out in triplicate, and the average values were reported.

$$sw = \frac{m_t - m_0}{m_0} \times 100\% \quad (2)$$

where m_t represents the weight of swollen sample at time t, m_0 is the weight of dried sample, respectively.

Results and discussion

In order to characterize the nanostructure of the vinyl-modified silica nanoparticles (VSNPs), we carried out the dynamic light scattering experiment on suspension as shown in Fig. 1. FT-IR was also carried out after drying the suspension as shown in Fig. 2. As shown in Fig. 1, the particle size of silica in the system was about 456 nm. It can be seen that the silica is in the nanoscale. In Fig. 2, the strong and wide absorption band at 1042 cm^{-1} can be ascribed to the Si–O–Si antisymmetric stretching. The peaks at 544 and 766 cm^{-1} can be attributed to Si–O symmetric stretching vibration. The peak at 1603 cm^{-1} resulted from the C=C double bond stretching

Table 1 Sample number and composition of gel prepared

Sample	PVA	PVA/%	AM/g	Silica/%[1]	Posttreatment method
PVA1799-freeze	1799	15	3	1.5	Freeze-thaw
PVA1799-annealing	1799	15	3	1.5	Annealing-swelling
PVA105-freeze	105	25	3	1.5	Freeze-thaw
PVA105-annealing	105	25	3	1.5	Annealing-swelling

The percentage by mass of silica in solution to acrylamide monomer

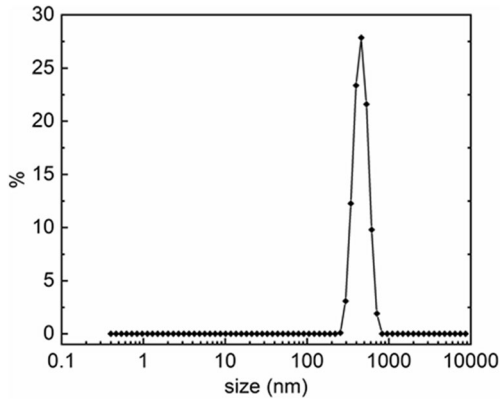

Fig. 1 Particle size distribution of silica dispersion

vibration. The results indicated the nanostructure of the vinyl-modified silica nanoparticles (VSNPs).

The composite interpenetrating gels with different post-treatment methods were tested by X-ray diffraction to characterize the crystallization of the composite gels. PVA1799-based gel without posttreatment was selected as control, and the corresponding XRD spectra were obtained as shown in Fig. 3. The distribution map shows that each sample had a wide peak at 2 θ≈18–21°, and there was a weak peak at 2 θ≈41 °. This was caused by the characteristic diffraction reflection of crystalline PVA. It can also be observed that the control sample showed a peak at 2 θ≈20°, the hydrogel treated by freeze-thaw method had a peak at 2 θ≈20°, and the hydrogel treated by annealing-swelling method had a peak at 2 θ≈21°, which may be due to the diffraction of PVA crystal plane formed by the intermolecular interference between PVA chains [41]. The results showed that the orderliness of PVA molecular chains was not affected by the formation and crosslinking of acrylamide network in the process of polymerization. The crystallization degree of the three samples can be calculated according to the formula as below:

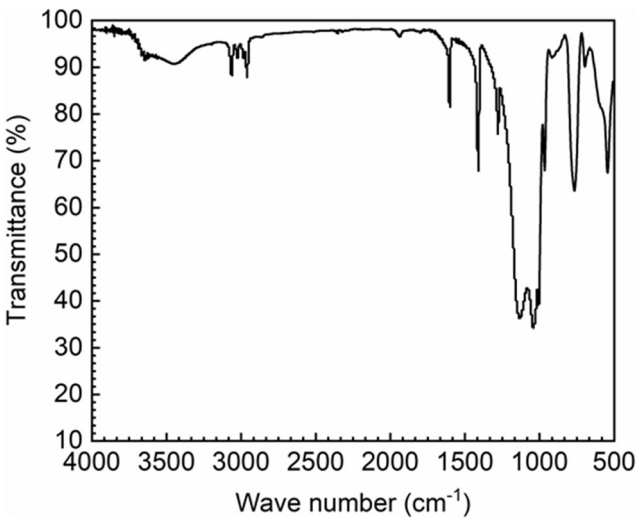

Fig. 2 FI-IR spectra of the dried VSNPs suspension

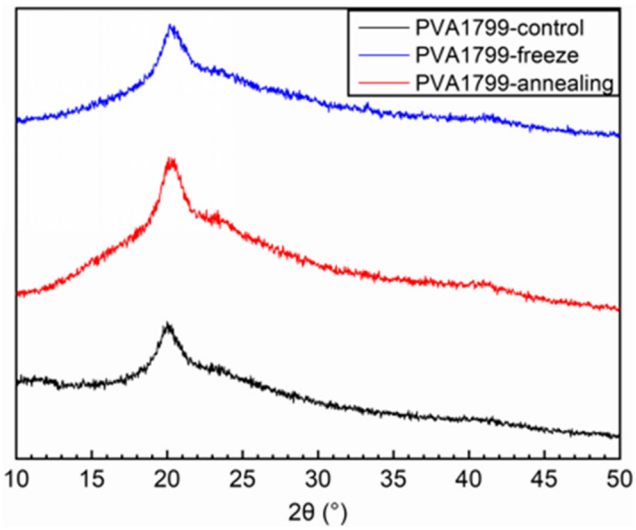

Fig. 3 XRD spectra of PVA-1799 hydrogels with different posttreatment

$$X_c = \frac{A_c}{A_c + A_a} \times 100\% \quad (3)$$

where A_c represents the area of the crystallization region. A_a represents the area of the amorphous region. Based on the equation, the crystallization degree of PVA-1799-control, PVA-1799-freeze, and PVA-1799-annealing were calculated to be 20.7%, 33.5%, and 39.0%, respectively. The crystallization degree of PVA was improved to a certain extent in the process of post-treatment, i.e., freeze-thawing and annealing-swelling, which resulted from the more intense intermolecular hydrogen bonding between PVA chains. Also, annealing-swelling method can increase the crystallization degree of PVA more obviously than freeze-thaw cycle. The enhancement in crystallization degree of anneal-swelling could be explained as follows: when being annealed, the elevated temperature contributed the mobility of the PVA chains, which generated a higher density of crystallites.

The nanocomposite interpenetrating hydrogels, including untreated, treated by freeze-thaw, and annealing swelling method, were further observed by scanning electron microscope (SEM) to investigate the network morphology (Fig. 4a–f). Typical porous structures could be seen for three samples, which were formed by the loss of water molecule sublimation in the process of freeze-drying. The untreated gel showed a porous structure with pore size of 3~4 μm. When treated by a freeze-thaw cycle, the composite interpenetrating gel shrank with a pore size of 2–2.5 μm. The denser network structure of freeze-thaw–treated gels originated mainly from the promoted hydrogen bonding of PVA chains. It should be mentioned that the anneal-swelling sample showed a hierarchical structure with the large micropore framework (~ 2.5 μm) interconnected by the nanopores (~ 500 nm). Moreover, some PVA microaggregates could be observed in Fig. 4e, which was not seen for untreated and freeze-thaw–

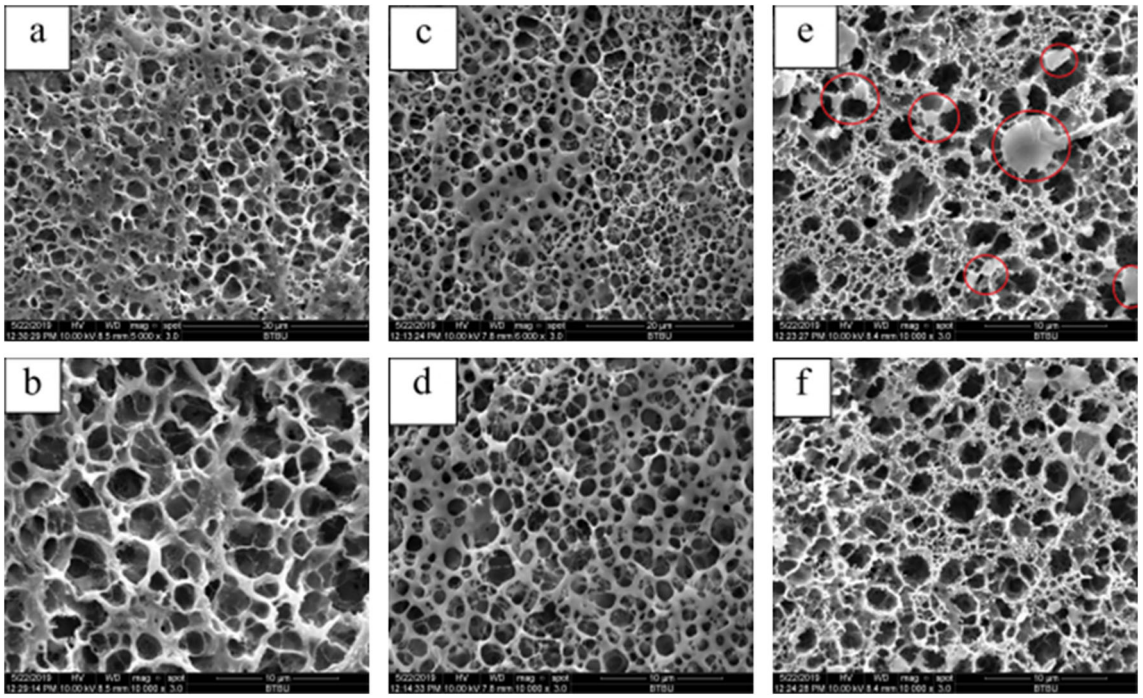

Fig. 4 Electron microscopic photos of nanocomposite interpenetrating gels, **a**, **b** PVA 1799-control, **c**, **d** PVA 1799-freeze, **e**, **f** PVA 1799-annealing

treated gels. These PVA crystallites probably resulted from the increased mobility of PVA molecular chains and more intense hydrogen bonding in annealing-swelling process. The morphological observations were in good agreement with XRD results as shown in Fig. 3.

The effect of posttreatment and PVA molecular weight on mechanical properties of nanocomposite interpenetrating hydrogels were investigated in detail. The tensile properties and typical stress-strain curves are shown in Figs. 5 and 6. The mechanical results showed that the posttreatment had a pronounced effect on the nanocomposite interpenetrating hydrogel. Take PVA-1799 based samples as an example. The tensile strength of PVA-1799 control sample was 0.40 MPa with the elongation at break of 501% (Fig. 5). The tensile properties of the composite gel after posttreatment were greatly improved. After freeze-thaw treatment, the tensile strength was raised by about 125% from 0.40 to 0.90 MPa, and the elongation at break increased insignificantly to approximately 585%. This was because molecular chains were frozen and many hydrogen bonds were produced between crosslinked networks during freezing. Hydrogen bond as a kind of interaction made the whole network structure more closely connected and the mechanical strength was improved. When thawing, due to the increase of temperature, the mobility of molecular chain increased, and more microcrystals were produced at the same time. This process also enhanced the interaction between molecules and further improved the mechanical strength. Compared with freeze-thaw method, the anneal-swelling method exerted a more pronounced effect on improving the tensile strength of PVA-1799-incorporated nanocomposite interpenetrating gels. As shown in Fig. 5, the tensile strength of PVA-1799-annealing reached 2.0 MPa, which was about four times that of the control sample. The promoted tensile strength could be explained as follows: when annealed at high temperature, the mobility of PVA chain were improved and thus more microcrystals were produced, which made the crystallinity of the composite gels larger than that of freeze-thaw–treated sample. Therefore, the annealed composite gel was stronger than the composite gel treated by freeze-thaw method. However, the elongation at break of PVA 1799 annealing decreased significantly to about 245%. It indicated that the toughness of the annealed composite gels was

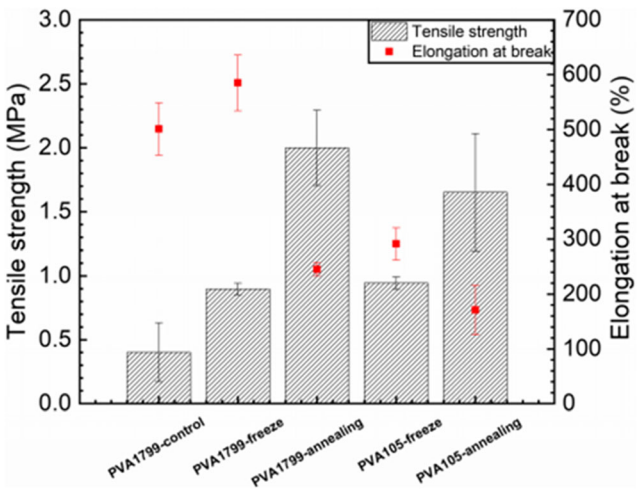

Fig. 5 Tensile properties of nanocomposite interpenetrating gels with different posttreatment methods and PVA molecular weights

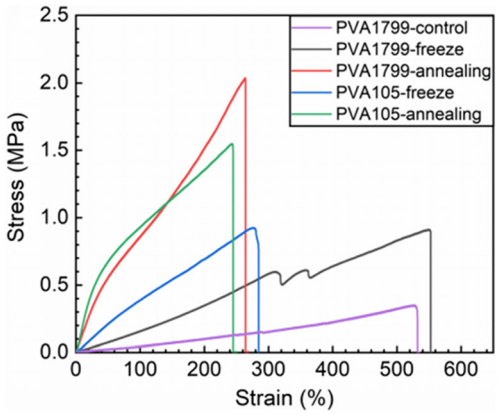

Fig. 6 Stress-strain curves of nanocomposite interpenetrating gels with different post-treatment methods PVA molecular weights

reduced. The annealing caused the PVA to produce the crystal microdomains, and the physical crosslinking of the PVA chain was promoted. Therefore, a physicochemical double network structure was formed in the composite gels. In this network, flexible and extensible networks were included in a rigid and brittle network and thus formed a layer of "brittle skin", which led to the reduced extension at break [42].

The effect of the posttreatment on the tensile properties also depended greatly on the molecular weight of PVA as shown in Fig. 7. For freeze-thaw method, PVA 1799-freeze and PVA 105-freeze hydrogels showed tensile strength of 0.90 and 0.95 MPa with 585 and 292% the elongation at break, respectively. On the other hand, the tensile strength of PVA 1799 annealing and PVA 105 annealing was 2.00 and 1.65 MPa with elongation of 245 and 171%, respectively. In other words, freeze-thaw cycle was more effective in elevating the tensile strength of PVA105 freeze gel, while producing a more pronounced influence on improving the elongation at break of PVA 1799 freeze gel. This may arise from the differed polymer chain length of PVA 1799 and PVA 105. For PVA 1799, the polymer chain length was higher, which tended to form intramolecular entanglement and intramolecular hydrogen bonding on freeze-thaw cycle. The intermolecular hydrogen bonding was reduced; therefore, the network was less close-packed to show a lowered tensile strength. On other hand, the longer chain of PVA 1799 can be stretched to a more extent and showed a higher elongation. It can also be found that annealing-swelling process can raise the tensile property of PVA 1799–based gels more effectively than freeze-thaw cycle method. Upon annealing, the intramolecular hydrogen bonding between PVA 1799 chains will greatly be disintegrated at elevated temperature. A large amount of intermolecular hydrogen bonding will be formed, and the aligned chains would result in a microcrystal zone. The increased crystals could serve as physical crosslinkers and enhance the tensile properties effectively.

Hydrogels with high strength and good toughness generally have obvious energy dissipation, which is of great importance in practice. In view of this, cyclic tensile loading–unloading was conducted for samples. There was a difference between the energy absorbed by tension and the energy released by springback. By calculating the difference between them, that is, the area surrounded by the formed energy loss ring, the dissipated energy can be obtained. The typical cyclic curves and calculated energy were illustrated in Fig. 7. At a 100% strain, the dissipated energy of PVA 1799 freeze, PVA 1799 annealing, PVA 105 freeze, and PVA 105 annealing were 0.0318, 0.201, 0.0688, and 0.789 MJ/m^3, respectively, as shown in Fig. 7b. It was interesting to find that dissipated energies of PVA 105–included samples were higher than that of PVA 1799–incorporated hydrogels at a 100% strain for both posttreatments. The reason may be as follows: when being stretched, PVA 105 with short chains can be rapidly stretched to its extreme at a lower strain, which could dissipate energy more effectively in a short stretching distance. Therefore, both PVA 105 freeze and PVA 1799 annealing samples exhibited higher dissipated energies. The trend in loading–unloading cycle was in good correspondence with the stress-strain curves in Fig. 6.

The nanocomposite interpenetrating gels showed good self-recovery and an obvious draw-inducing toughening effect. As shown in Fig. 8a, after being redrawn at intervals of 30 min, the tensile strength of PVA 1799 freeze and PVA 105

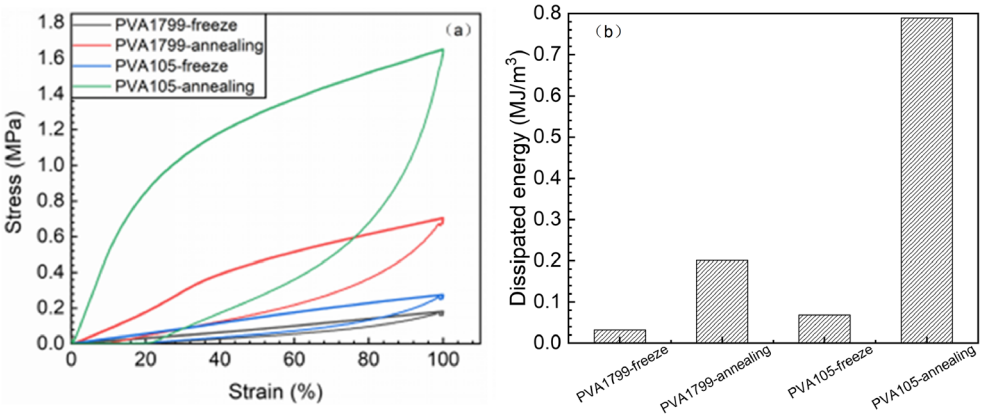

Fig. 7 **a** Tensile loading-unloading curves and **b** dissipated energy of composite gels with different posttreatment methods and PVA molecular weights

freeze samples increased from 0.18 and 0.28 MPa to 0.37 and 0.60 MP respectively. The fracture energy increased from 0.032 and 0.069 to 0.15 and 0.12 MJ/m^3, respectively (Fig. 8b). After resting for 60 min, the values of tensile strength and fracture energy of PVA 105 freeze were further increased to 0.38 MPa and 0.24 MJ/m^3. For PVA 1799 freeze sample, the tensile strength and fracture energy were 0.55 MPa and 0.21 MJ/m^3. This could be ascribed to the reversible physical crosslinking of the gels, which could be reversibly disintegrated and formed when being stretched. In the whole process of stress, the crystal region of PVA was parallel to the orientation of tensile direction. This orientation was maintained after relaxation, so the mechanical strength of the hydrogel was significantly improved during the two tensile periods [43].

In order to determine the water absorption properties of the composite gel, the swelling kinetics of PVA control sample and samples with posttreatment was recorded. The swelling kinetic curves of the composite gel with different posttreatment methods were shown in Fig. 9. As can be seen from the diagram, the composite gels absorbed water rapidly in a short period of time, and then the water absorption rate became very slowly over time. The swelling rates differed with the posttreatment methods. Take PVA 1799 included gels as an example. The swelling ratio of PVA 1799 freeze was slightly lower than that of the untreated composite gel, which was 370% (the swelling ratio of the untreated composite gel was 420%). The swelling rate of PVA 1799 annealing decreased to 275%. That is, the swelling capacities of the nanocomposite interpenetrating gels with both posttreatment were lower than the control sample. This was because a large number of interchain and intrachain hydrogen bonds formed in freeze-thaw cycle, which resulted in a dense network structure. It was difficult for water molecules to diffuse into the network. Compared with freeze-thaw method, drying and water removal made the network structure of PVA concentrated in the composite gel, and the pore structure of annealing-swelling method was more compact than that of freeze-thaw method. The water absorption performance of the composite gel is

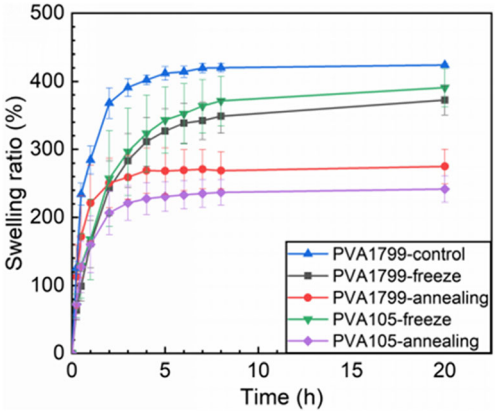

Fig. 9 Swelling kinetics of the nanocomposite gel with different posttreatment methods and PVA molecular weights

related to the pore size of its network structure. The gel with smaller pore size generally showed a lower swelling ratio. Therefore, the swelling rate of the treated composite gel showed decreased swelling ratios than the untreated gel.

In addition, the swelling kinetics of hydrogel was simulated by Fickian model and Schott model, respectively, and the swelling rate constant K and the fitting equilibrium swelling rate W_e, were calculated as shown in Table 2.

In order to study the diffusion model of hydrogel, the initial swelling data were fitted to $W/W_e \leq 0.5$ by Fickian model, and the formula is

$$\frac{W}{We} = Kt^{n} \tag{4}$$

where K is the swelling rate constant, n is the characteristic index, W is the swelling rate at t time, and W_e is the equilibrium swelling ratio. The plot of lg(W/W_e)against lg$t$ is shown in Fig. 10. Linear relations can be obtained for the gels. The values of n and K can be calculated from the slope and intercepts of the lines as shown in Table 2.

The calculation results showed that the swelling rate of the hydrogel treated by freeze-thaw method was low at the initial stage, which may be due to the decrease of the hydrophilic groups exposed to the surface in the posttreatment process,

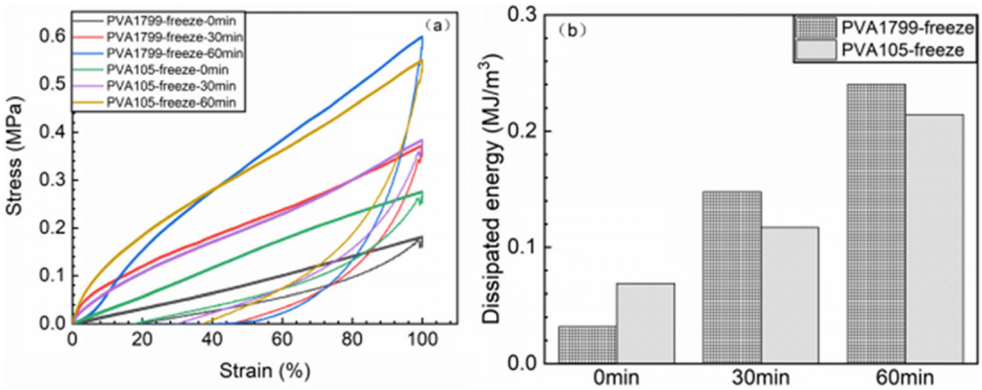

Fig. 8 **a** Three successive loading–unloading cycling test of freeze-thaw–treated samples at a strain of 100% with 30 min resting between two tests, **b** the time-dependent recovery of dissipated energy

Table 2 Results obtained from linear regression of the different kinetics equations

Sample	Fickian model			Schott model		
	n	K (g g^{-1}·min$^{-0.3}$)	R^2	W_e (fitting data, g/g)	W_e (experimental data, g/g)	R^2
PVA 1799 freeze	0.6695	8.4429	0.9991	3.413	3.725	0.9992
PVA 1799 annealing	0.4836	9.0571	0.9800	3.226	2.752	0.9999
PVA 1799 control	0.5860	8.8156	0.9175	4.651	4.242	0.9996
PVA 105 freeze	0.6280	8.5415	0.9498	2.994	3.908	0.9993
PVA 105 annealing	0.5744	8.8247	0.9437	2.604	2.418	0.9998

which leads to the slow absorption of water, while the high initial swelling rate of the hydrogel treated by annealing swelling method may be due to the fact that more hydrophilic groups are exposed to the surface. Because of the secondary kinetics in the later stage of swelling process, Fickian model cannot simulate the swelling rate and can be simulated by Schott model.

For Schott model, the swelling rate the swelling rate at any time was expressed as follows:

$$\frac{dW}{dt} = K(We-W)^2 \tag{5}$$

where W is the swelling ratio of the hydrogel at time t, W_e is the swelling ratio of the hydrogel at equilibrium, and K is the rate constant. The integration form in scope [0, t] and [0, W_t] can be represented as follows:

$$\frac{1}{We-W} = Kt + \frac{t}{We} \tag{6}$$

and then, it could be reorganized to obtain a linear form:

$$\frac{t}{W} = \frac{1}{K \cdot We^2} + \frac{t}{We} \tag{7}$$

By plotting a graph (Fig. 11) of t/W versus t, a straight line with a slope of $1/W_e$ and an intercept of $1/(K \cdot W_e^2)$ could be obtained. From this plot, the swelling capacity (W_e) and the swelling rate constant (K) could be evaluated by the slope and intercept.

The values of R^2 of all the hydrogels were higher than 0.99 (Table 2), suggesting that the experimental data were well fitted by the Schott model. The calculated results of the model were in good agreement with the experimental data, which indicated that the previous discussion and analysis are valid.

Conclusions

In summary, a mechanically strong nanocomposite interpenetrating hydrogel was fabricated, in which VSNPs were included as nanocrossliners and PVA hydrogen bonding and microcrystals served as the reversible physical linkage. The posttreatment methods and PVA molecular weight played important roles on the mechanical and swelling properties on the nanocomposite interpenetrating gels. Annealing-swelling process could increase the crystallization degree of PVA to a greater extent, thus having a more prominent influence on elevating the tensile strength of nanocomposite interpenetrating hydrogels. Hydrogels with lower PVA molecular weight could be stretched in a short distance to dissipate higher energy, so they displayed a higher tensile strength than that of the gels with higher PVA molecular weight within a low strain range, i.e., 100%. The swelling kinetic study

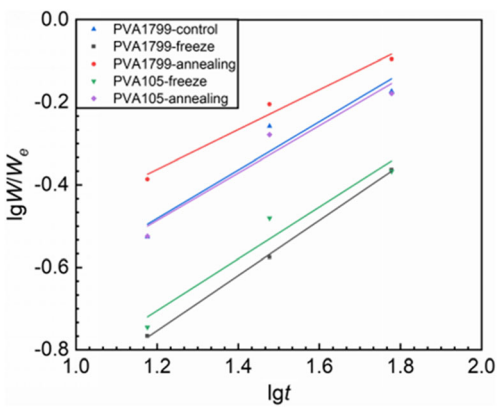

Fig. 10 Plots of lg(W/W_e) against lg$t$ for the nanocomposite hydrogels

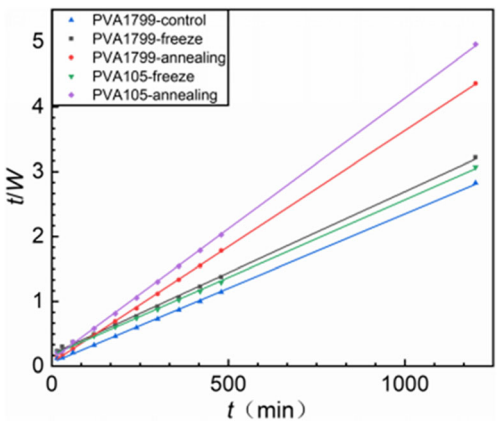

Fig. 11 Plots of t/W against t for the nanocomposite hydrogels

revealed that the swelling behaviors of nanocomposite interpenetrating hydrogels followed the pseudo-second-order dynamic equation.

Funding We acknowledge financial support from the National Nature Science Foundation of China (Nos. 21104040, 51473007) and Construction of Scientific Research Team of Beijing Technology and Business University (No. 19005902015).

Compliance with ethical standards

Conflict of interest The authors declare that they have no conflict of interest.

References

1. Chang G, Chen Y, Li Y, Li S, Huang F, Shen Y, Xie A (2015) Self-healable hydrogel on tumor cell as drug delivery system for localized and effective therapy. Carbohydr Polym 122:336–342
2. Han XD, Zhang W, Yu K, Jia QM, Shan SY, Su HY (2017) Advances in the application of magnetic hydrogels as drug carriers. Mater Rev 31(15):30–35
3. Chen C, Zhang T, Dai B, Zhang H, Chen X, Yang J, Liu J, Sun D (2016) Rapid fabrication of composite hydrogel microfibers for weavable and sustainable antibacterial applications. ACS Sustain Chem Eng 4:6534–6542
4. Lee KY, Mooney DJ (2001) Hydrogels for tissue engineering. Chem Rev 101(7):1869–1879
5. Wang WB, Kang YR, Wang AQ (2013) One-step fabrication in aqueous solution of a granular alginate-based hydrogel for fast and efficient removal of heavy metal ions. J Polym Res 20:101
6. Ryzhuk V, Zeng XX, Wang X (2017) Human amnion extracellular matrix derived bioactive hydrogel for cell delivery and tissue engineering. Mater Sci Eng C 85:191–202
7. Appel EA, del Barrio J, Loh XJ, Scherman OA (2012) Supramolecular polymeric hydrogels. Chem Soc Rev 41(18): 6195–6214
8. Yang W, Bai T, Carr LR (2012) The effect of lightly crosslinked poly(carboxybetaine) hydrogel coating on the performance of sensors in whole blood. Biomaterials 33(32):7945–7951
9. Sorber J, Steiner G, Schulz V (2008) Hydrogel-based piezoresistive pH sensors: investigations using FT-IR attenuated total reflection spectroscopic imaging. Anal Chem 80(8):2957–2962
10. Ito K (2007) Novel cross-linking concept of polymer network: synthesis, structure, and properties of slide-ring gels with freely movable junctions. Polym J 39:489–499
11. Peng L, Zhang HJ, Feng AC, Huo M, Wang ZL, Hu J, Gao WP, Yuan JY (2015) Electrochemical redox responsive supramolecular self-healing hydrogels based on host–guest interaction. Polym Chem 6:3652–3659
12. Peak CW, Wilker JJ, Schmidt G (2013) A review on tough and sticky hydrogels. Colloid Polym Sci 291(9):2031–2047
13. Tao LL, Heikki T, Henrik T (1999) Effect of hydrophobicity of a drug on its release from hydrogels with different topological structures. J Appl Polym Sci 73(6):1031–1039
14. Daniele MA, Adams AA, Naciri J (2014) Interpenetrating networks based on gelatin methacrylamide and PEG formed using concurrent thiol click chemistries for hydrogel tissue engineering scaffolds. Biomaterials 35(6):1845–1856
15. Haraguchi K, Takehisa T, Fan S (2002) Effects of clay content on the properties of nanocomposite hydrogels composed of poly(N-isopropylacrylamide) and clay. Macromolecules 35:10162–10171
16. Zhu MF, Liu Y, Sun B, Zhang W, Liu XL, Yu H, Zhang Y, Kuckling D, Adler HP (2006) A novel highly resilient nanocomposite hydrogel with low hysteresis and ultrahigh elongation. Macromol Rapid Commun 27:1023–1028
17. Kostina NY, Sharifi S, Pereira AS, Michálek J, Grijpma DW, Rodriguez-Emmenegger C (2013) Novel antifouling self-healing poly(carboxybetaine methacrylamide-co-HEMA) nanocomposite hydrogels with superior mechanical properties. J Mater Chem B 1:5644–5650
18. Li ZY, Su YL, Xie BQ, Wang HL, Wen T, He CC, Shen H, Wu DC, Wang DJ (2013) A tough hydrogel–hydroxyapatite bone-like composite fabricated in situ by the electrophoresis approach. J Mater Chem B 1:1755–1764
19. Hu J, Kurokawa T, Hiwatashi TK, Nakajima T, Wu ZL, Liang SM, Gong JP (2012) Structure optimization and mechanical model for microgel-reinforced hydrogels with high strength and toughness. Macromolecules 45:5218–5228
20. Hu J, Hiwatashi K, Kurokawa T, Liang SM, Wu ZL, Gong JP (2011) Microgel-reinforced hydrogel films with high mechanical strength and their visible mesoscale fracture structure. Macromolecules 44:7775–7781
21. Gao GR, Du GL, Cheng YJ, Fu J (2014) Tough nanocomposite double network hydrogels reinforced with clay nanorods through covalent bonding and reversible chain adsorption. J Mater Chem B 2:1539–1549
22. Aranaz I, Martínez-Campos E, Nash ME, Tardajos MG, Reinecke H, Elvira C, Ramos V, López-Lacomba JL, Gallardo A (2014) Pseudo-double network hydrogels with unique properties as supports for cell manipulation. J Mater Chem B 2:3839–3848
23. Yin HY, Akasaki T, Sun TL, Nakajima T, Kurokawa T, Nonoyama T, Taira T, Saruwatari Y, Gong JP (2013) Double network hydrogels from polyzwitterions: high mechanical strength and excellent anti-biofouling properties. J Mater Chem B 1:3685–3693
24. Pan T, Zhang Y, Wang CH, Gao H, Wen BY, Yao BQ (2020) Mulberry-like polyaniline-based flexible composite fabrics with effective electromagnetic shielding capability. Compos Sci Technol 188:107991
25. Qiu S, Ge NJ, Sun DK (2016) Synthesis and characterization of magnetic polyvinyl alcohol (PVA) hydrogel microspheres for the embolization of blood vessel. IEEE Trans Biomed Eng 63(4):730
26. Rodrigues IR, Forte MMC, Azambuja DS (2007) Synthesis and characterization of hybrid polymeric networks (HPN) based on polyvinyl alcohol/chitosan. React Funct Polym 67(8):708–715
27. Pritchard JG, Fung YLLC (1976) Determination of vicinal hydroxyl groups in poly(vinyl alcohol) (pva). Talanta 23(3):237–239
28. Bunn CW (1948) Crystal structure of polyvinyl alcohol. Nature 161(4102):929–930
29. Bodugoz-Senturk H, Macias CE, Kung JH, Muratoglu OK (2009) Poly (vinyl alcohol)-acrylamide hydrogels as load-bearing cartilage substitute. Biomaterials 30:589–596
30. Park KR, Nho YC (2003) Synthesis of PVA/PVP hydrogels having two-layer by radiation and their physical properties. Radiat Phys Chem 67:361–365
31. Mansur HS, Sadahira CM, Souza AN, Mansur AAP (2008) FTIR spectroscopy characterization of poly (vinyl alcohol) hydrogel with different hydrolysis degree and chemically crosslinked with glutaraldehyde. Mater Sci Eng C 28:539–548
32. Liu Y, Vrana N, Cahill P, Mcguinness GB (2009) Physically crosslinked composite hydrogels of PVA with natural macromolecules: structure, mechanical properties, and endothelial cell compatibility. J Biomed Mater Res B Appl Biomater 90:492–502
33. Cha WI, Hyon SH, Oka M (1996) Mechanical and wear properties of poly(vinyl alcohol) hydrogels. Macromol Symp 109(1):115–126
34. Ou KK, Dong X, Qin CL, Ji XN, He JX (2017) Properties and toughening mechanisms of PVA/PAM double-network hydrogels

prepared by freeze-thawing and anneal-swelling. Mater Sci Eng C 77:1017–1026
35. Zhang HJ, Wang X, Huang HX, Yang B, Wang C, Sun H (2019) Nanocomposite interpenetrating hydrogels with high toughness and good self-recovery. Colloid Polym Sci 297:821–830
36. Gupta S, Goswami S, Sinha A (2012) A combined effect of freeze-thaw cycles and polymer concentration on the structure and mechanical properties of transparent PVA gels. Biomed Mater 7(1): 015006
37. Martens P, Blundo J, Nilasaroya A (2007) Effect of poly(vinyl alcohol) macromer chemistry and chain interactions on hydrogel mechanical properties. Chem Mater 19(10):2641–2648
38. Temenoff JS, Athanasiou KA, Lebaron RG (2002) Effect of poly(-ethylene glycol) molecular weight on tensile and swelling properties of oligo(poly(ethylene glycol) fumarate) hydrogels for cartilage tissue engineering. J Biomed Mater Res 59(3):429–437
39. Shi FK, Wang XP, Guo RH, Zhong M, Xie XM (2015) Highly stretchable and super tough nanocomposite physical hydrogels facilitated by the coupling of intermolecular hydrogen bonds and analogous chemical crosslinking of nanoparticles. J Mater Chem B 3:1187–1192
40. Zhong M, Liu XY, Shi FK, Zhang LQ, Wang XP, Cheetham AG, Cui HG, Xie XM (2015) Self-healable, tough and highly stretchable ionic nanocomposite physical hydrogels. Soft Matter 11:4235–4241
41. Yuan F, Ma M, Lu L (2017) Preparation and properties of polyvinyl alcohol (PVA) and hydroxylapatite (HA) hydrogels for cartilage tissue engineering. Cell Mol Biol 63(5):32
42. Wu XY, Huang SW, Zhang JT, Zhuo RX (2004) Preparation and properties of physical cross-linked polyvinyl alcohol/hydroxyl-terminated polyamide-amine dendritic polymer hydrogels. Chem J Chin Univ 02:382–384
43. Wang MB, Li YB, MOU YH (2006) Study on the structure and properties of nano hydroxylapatite polyvinyl alcohol hydrogels. Funct Mater 379:1477–1480